State-of-the art of acousto-optic sensing and imaging of turbid media

Steffen G. Resink
Albert C. Boccara
Wiendelt Steenbergen

State-of-the art of acousto-optic sensing and imaging of turbid media

Steffen G. Resink,[a] Albert C. Boccara,[b] and Wiendelt Steenbergen[a]
[a]MIRA Institute for Biomedical, Technology and Technical Medicine University of Twente, Biomedical Photonic Imaging Group, P.O. Box 217, 7500 AE Enschede, the Netherlands
[b]Institut Langevin, ESPCI ParisTech, CNRS UMR 7587, 10 Rue Vauquelin, F-75231 Paris Cedex 05, France

Abstract. Acousto-optic (AO) is an emerging hybrid technique for measuring optical contrast in turbid media using coherent light and ultrasound (US). A turbid object is illuminated with a coherent light source leading to speckle formation in the remitted light. With the use of US, a small volume is selected,which is commonly referred to as the "tagging" volume. This volume acts as a source of modulated light, where modulation might involve phase and intensity change. The tagging volume is created by focusing ultrasound for good lateral resolution; the axial resolution is accomplished by making either the US frequency, amplitude, or phase time-dependent. Typical resolutions are in the order of 1 mm. We will concentrate on the progress in the field since 2003. Different schemes will be discussed to detect the modulated photons based on speckle detection, heterodyne detection, photorefractive crystal (PRC) assisted detection, and spectral hole burning (SHB) as well as Fabry-Perot interferometers. The SHB and Fabry-Perot interferometer techniques are insensitive to speckle decorrelation and therefore suitable for *in vivo* imaging. However, heterodyne and PRC methods also have potential for *in vivo* measurements. Besides measuring optical properties such as scattering and absorption, AO can be applied in fluorescence and elastography applications. © *2012 Society of Photo-Optical Instrumentation Engineers (SPIE).* [DOI: 10.1117/1.JBO.17.4.040901]

1 Introduction

Noninvasive diagnostic imaging technologies to detect cancer and other diseases come in a wide variety. Most of these technologies like MRI and x-ray lack optical contrast that can be beneficial for detection of small lesions without the use of contrast agents or ionizing radiation.[1]

Optical techniques such as optical coherence tomography (OCT) and diffuse optical tomography (DOT) show good contrast, but the measuring depth and resolution, respectively, are limited by the strong scattering of tissue. Measuring with high resolution at penetration depths larger than 1 mm is challenging due to the high optical scattering that induces a strong attenuation of ballistic photons. These optical techniques are noninvasive and use nonionizing radiation in contrast to x-ray. The absorption coefficient of light is wavelength dependent, making spectroscopy possible, which can be used to determine blood oxygenation levels.

Ultrasound (US) in the few MHz ranges has a scattering coefficient two to three orders of magnitude[2] less than light, which comparatively allows for superior penetration depth while retaining spatial resolution. There is, however, a drawback in which US lacks the benefits of optical contrast.

Two hybrid forms of imaging techniques that use the interplay of sound and light are emerging: acousto-optics (AO) and photoacoustics (PA). These techniques combine the high resolution of US with the strong contrast found in purely optical techniques while remaining noninvasive in nature.

The principle of PA relies on a light pulse irradiating an object of interest. Some parts of the object will absorb this light and will expand thermoelastically. The resulting expansion causes an US wave that is detected by a broadband US probe.[3] The resolution is limited by the light pulse duration, the acoustic tissue properties, and the frequency transfer function of the US detection. The higher the detected frequencies the higher the resolution will be. The longer the light pulse duration, the lower the frequencies of the PA signal and the lower the resolution. The acoustic attenuation typically increases with the acoustic frequency, therefore the resolution deteriorates with increasing depth. Typical resolutions are micrometers for PA microscopy with a measuring depth of millimeters[4] and up to millimeters for PA mammography[5] on a measuring depth of centimeters. While the resolution is achieved by the ultrasound, the contrast is provided by optical absorption; the amount of detected pressure depends on the optical absorption inside the object under investigation.

A second technique that combines ultrasound and light is AO. The possibility of tagging light was investigated by Marks et al.[6] Leutz and Maret,[7] Wang et al.[8] and by a patent from Dolfi and Micheron.[9] The sample is illuminated with coherent light, and hence a speckle pattern is formed due to complete randomization of the phases of the electric field of the light escaping from the medium.

To measure only photons that traveled through a volume of interest, ultrasound (US) is employed to encapsulate this bounded region from the characteristic focal zone of the transducer. The photons passing through the US focus will be frequency shifted or, in other words, phase modulated and

Address all correspondence to: S. G. Resink, MIRA Institute for Biomedical. Technology and Technical Medicine University of Twente, Biomedical Photonic Imaging Group, P.O. Box 217, 7500 AE Enschede, the Netherlands. Tel.: +0031627282050; E-mail: s.g.resink@utwente.nl.

thus tagged by the US. A variety of tagging strategies have been developed, along with different detection schemes to find the tagged photons in the sea of untagged photons. The tagged photons detected after exiting the medium provide information on the optical properties present in the vicinity of the volume of interest. When the tagging zone is placed in a tissue volume with high optical absorption compared with the rest of the object, less tagged photons will be detected. This in contrast with when the ultrasound focus is placed in the neighboring tissue. In this review we describe the progress made in AO imaging since the previous review by Wang[10] in 2003: theoretical models, the detection methods to detect the tagged photons, and applications of AO imaging. For further reading, are view by Elson et al.[11] is also focusing on the detection methods, scanning, and applications. They give, however, no equations from the models in the modeling section.

In recent years, considerable improvements in AO have been realized. Some groups developed a method to use AO in a reflection mode setup.[12–15] Others[16,17] investigated the decay of the modulation of the signal as function of the imaging depth and enhancement of AO with micro bubbles, which can be important in the development of new applications.

2 Acousto-Optic Tagging Mechanisms

Light can be modulated in a scattering medium using ultrasound by sixdifferent mechanisms. The relative influence of each of these mechanisms depends on the optical properties of the sample and light source and the acoustic properties of sample and transducer.

The first two mechanisms (see Fig. 1) require light to have a sufficient coherence length. The first mechanism relies on the modulation of the optical path length. The scatterers inside the medium are assumed to oscillate with the US frequency at the US focus due to the pressure wave. The optical path length varies with the distance between the scatterers, and therefore the speckle pattern will vary with the applied US frequency.[7] This mechanism is thus equivalent to Doppler scattering and relies on coherent light with a long coherence length to obtain a clear speckle pattern. The mean optical path length is, depending on the optical properties, in the order of 10 to 30 cm for an object with a thickness of 3 cm.[18,19] The coherence length must be at least in the same order of magnitude. Leutz and Maret[7] have developed a theory that partially modeled this mechanism. The theory is only valid when the mean free path is much greater than the light wavelength, and the particle displacement must be much smaller than the light wavelength. Unfortunately, the second mechanism is dominant in this case.

The second mechanism is based on refractive index variations due to the acoustic pressure wave. As a result the
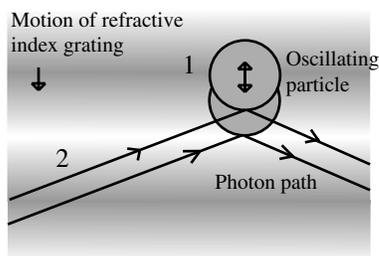

Fig. 1 Coherent modulation mechanisms: oscillation of scattering particles modulate the photon optical path length (1) and optical path length variation due to refractive index changes (2).
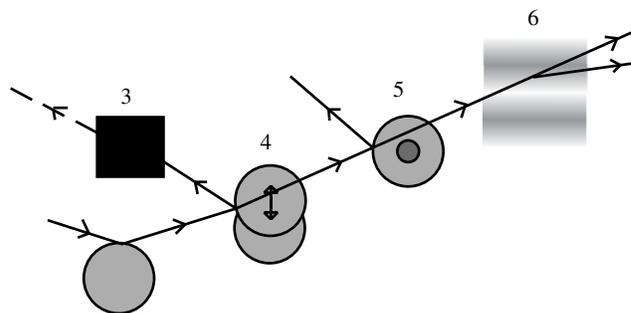

Fig. 2 Incoherent modulation mechanisms: absorption modulation (3), variation of the position of scattering particles (4), scattering particle cross-section variation (5), and variation in refractive index leading to Bragg diffraction patterns (6).

optical path lengths, and therefore the phases, are modulated. Consequently, the intensity of the resulting speckle pattern is also modulated.[10]

The relative influence of particle vibration and refractive index changes on the induced phase change depends on the optic and acoustic properties of the medium and the used waves.[20–22] Properties such as scattering coefficient and the wavelengths of the ultrasound and probing light change the relative influence of the first and second mechanisms. The strengths of both mechanisms are comparable up to a critical point from where the acoustic wave vector becomes larger than a critical fraction of the mean free path of the photons and the second mechanism becomes dominant.[20]

The otherfourmechanisms (see Fig. 2) are incoherent phenomena. As a result of US associated local pressure variations, the medium is continuously locally compressed and decompressed. Local optical properties such as absorption (mechanism 3), position, and scattering cross-section of scattering particles (4 and 5) and the refractive index[6] of the medium will oscillate with the US frequency due to variations in density.[10] The four mechanisms each result in variation of the fluence distribution inside the object. In many situations the associated variation in signal strength is too low to be measured.[10] However, Krishnan[23] proposed a theory that fluorescent light is modulated by the gradient of the refractive index by an acoustic lens effect (mechanism 6). Kobayashi et al.[24] showed the feasibility of detecting this modulated intensity in fluorescence.

3 Theoretical Modeling

To understand AO modulation, and to explore the relative importance of the above mechanisms for modulating the light, different theoretical models have been developed. Most models use the more classical approach of phase changes induced by ultrasound, as described by Secs. 3.2 and 3.3. A different approach used by Mahan et al.[25] is more from a quantum mechanics perspective. Here the fraction of tagged and untagged photons is calculated (see Sec. 3.1).

3.1 *Fraction of Tagged Light by Brillouin Scattering*

Mahan et al.[25] used the mechanism of refractive index changes due to the ultrasound to model the tagged light. The periodic refractive index changes causes Brillouin scattering of the photon stream. A small fraction of these photons will scatter inelastic and are frequency shifted with the US frequency. The intensity of the tagged photon stream is a fraction r of the untagged photon

stream. They start by deriving an expression for the signal strength of the untagged photons. Step two is calculating the fraction r for different geometries. For a slab with thickness d

$$r = \frac{3V_{US}g\mu_a\delta\mu_s}{2\pi d},$$ (1)

where the ultrasound is uniformly distributed this fraction is given by: where V_{US} is the volume of the ultrasound pulse, g the anisotropy factor, μ_a the absorption coefficient $\delta\mu_s$ the variation in scattering coefficient due to refractive index changes (tagging mechanism 2 and 5). This fraction of tagged photons is coupled to the signal strength for an AO measurement. The measured signal strength depends on this fraction and the type and quality of the setup. When this signal is compared with the noise, it can be decided whether there is enough signal for imaging purposes.

3.2 Theoretical Predictions of Observable Optical Quantities During US Modulation

The ultrasound modulation of light has been modeled for its consequence for two observable aspects of speckle patterns: temporal fluctuations and reduction of speckle contrast, which are coupled to one another. The modulation of the speckle pattern formed at the detector is often calculated by using the temporal autocorrelation function of the electric field. The intensity of a speckle consists of a large DC component and a smaller component, the one in which we are interested, that varies in time with the US frequency. Leutz et al.[7] and others[10,20,21,26,27] expressed this autocorrelation function as:

$$G_1(t) = \langle E(0)E^*(t)\rangle \quad = \int_t^\infty p(s)\langle E(t)E^*(t+\tau)\rangle ds \quad (2)$$

with $p(s)$ the distribution function of paths with length s through the sample and E_s the electric field. The < > denote averaging over time. This equation is related to the speckle power spectrum S through a Fourier transformation based on the Wiener-Khinchin theorem:

$$S(\omega) = \int_{-\infty}^\infty G_1(\tau)e^{i\omega\tau}d\tau,$$ (3)

where ω is relative to the optical frequency ω_0 and thus equal to the frequency of the oscillating speckles or beat frequency of the light.[10] Point-like scatterers are undergoing a collective motion due to the ultrasound and Brownian motion. The autocorrelation function length can be split in one part describing the exponential decay due to Brownian motion and a second part that describes the autocorrelation as a function of the periodic ultrasound wave. When both effects are assumed independent from the other then the properties of both factors can be explored separately.

The scatterers in the medium may tend to diffuse due to the Brownian motion. The single particle relaxation time is given by $\tau_0 = 1/Dk_0^2$ where D is the particle diffusion constant and k_0 the wave vector of the light. The autocorrelation of the electric field with a single path length will decay exponentially in time t according to:[7]

$$\langle E_s(0)E_s^*(t)\rangle_B = \exp\left(-\frac{2ts}{\tau_0 l}\right),$$ (4)

where l is the mean free path.

This decay time limits the time in which an accurate AO measurement can be performed in most situations. The Brownian motion can be neglected for time scales in the order of the cycle time of the ultrasound.[28] Wang[20,21] investigated the contribution of phase modulation by refractive index changes and scatterer displacement induced by the ultrasound. He concluded that both effects have a similar contribution up to a critical point. When the mean free paths of the photons between two scattering events become small compared with the acoustic wavelength, the second mechanism becomes increasingly more important. This was verified with a Monte Carlo simulation.[20]

Sakadžić et al.[26,29–31] and Wang[20] developed an analytical solution for this autocorrelation function Eq. (2), mostly focusing on the first two mechanisms. For a single pathlength s the contribution to the autocorrelation function is given by:[20]

$$\langle E_s(t)E_s^*(t+\tau)\rangle = \langle\exp[-i\Delta\phi(t+\tau)]\rangle,$$ (5)

where $\Delta\phi$ denotes the total phase shift of the light due to path length and refractive index variations and is thus a function of μ_s, Δn (mechanism 1 and 2) of the object. After some lengthy algebra[10,26] and the assumption of weak modulation, the modulation depth, defined as ratio of the intensity at the signal frequency and the unmodulated intensity,[10] is found to be proportional to the acoustic amplitude squared.[10] In general the maximum variation of the autocorrelation function will increase with increasing acoustic power and decrease with increasing US frequency while keeping the US power constant. Increasing the optical absorption coefficients will lead to a smaller variation according to:[22,26]

$$G_1(\tau) = \frac{\sin h\left(L_0\sqrt{\mu_a D^{-1}}\right)\sin h\left[z_0\sqrt{(S_u + S_B + \mu_a)D^{-1}}\right]}{\sin h\left(Z_0\sqrt{\mu_a D^{-1}}\right)\sin h\left[L_0\sqrt{(S_u + S_B + \mu_a)D^{-1}}\right]},$$ (6)

where L_0 the distance between the extrapolated slab boundaries, z_0 is the location of the isotropic light source, S_u the term due to ultrasound influence, S_B the term for Brownian motion, μ_a the absorption coefficient and D the diffusion constant.

The intensity and variation of the speckle contrast, which is related to the autocorrelation function, are derived by Zemp et al.[27] The statistical properties of this speckle pattern are derived from the autocorrelation function. The first order statistics describe the time average intensity and is approximately equal to $G_1(0)$. The second order statistics describe the variation in speckle contrast. The variation is approximately

$$\Delta C \approx \frac{\bar{s}}{4}\left(n_0 k_0\frac{P_0}{\rho v_a^2}\right)\eta^2\frac{v_a}{f_a}.$$ (7)

This variation is a function of the average optical pathlength $\bar{s}$, the optical index of refraction n_0, the magnitude of the optical wave vector k_0, the acoustic pressure P_0, the mass density of the medium ρ, the ultrasound velocity v_a, the elasto-optic coefficient η which has a value of approximately 0.32 and the acoustic frequency f_a. This equation is valid under the assumption of weak scattering i.e., $k_a l_{tr} \gg 1$ where k_a is the ultrasonic wave vector magnitude and l_{tr} is the transport mean free path. The model predicts a linear relation between

the acoustic power and the speckle contrast, which is verified experimentally in Ref. 27. All these theories assume homogeneous acoustic waves, except for Sakadžić et al.[29–31] in which localized acoustic waves were used.

3.3 Monte Carlo Simulations

Besides the analytical solutions Monte Carlo (MC) simulations are used to gain more insight into the principles of AO. These models simulate photon distributions inside the medium and include scattering and absorption of the light. One or more of the tagging mechanisms can be implemented, and the refractive index and scatterer motion can be modulated. The results of measurements and analytical models are often compared and tested with MC simulation results.[32–34] Wang[20] and others[33] developed and modified MC models for AO applications. Especially the model of Wang et al. is widely used in Biomed.Op. i.e.,[35,36] and is supported by an analytical model.[21,26,29,30]

Leung et al.[37] compared the speed of this model implemented on both central processing unit (CPU) and graphics processing unit (GPU, Nvidia GeForce 9800) with Compute Unified Device Architecture (CUDA). They found an increase in speed, depending on simulation settings and hardware, of a factor 72 for the CUDA implementation.

4 Detection of Tagged Photons

A detection technique must be able to distinguish the tagged or modulated photons from the untagged or unmodulated photons to obtain information from the US focus. Longer integration times will lead to higher signal-to-noise ratios. However, speckle decorrelation alters the speckle pattern and destroys the correlation of this pattern between the start and end of the detection time. Sources of speckle decorrelation are small changes in the optical paths inside the object, i.e., Brownian motion of scatterers and blood flow or muscular activity in living tissues. This decorrelation diminishes the detectability of tagged photons. Developed detection techniques can be divided in time- and frequency domain techniques.

4.1 Time-Based Methods

Wang et al.[8] measured light modulated at a US frequency of 1 MHz with a photomultiplier. The intensity of a single speckle will oscillate with the US frequency of 1 MHz, and this frequency is observed by recording the light flux with the photomultiplier tube. They used a 1.1-mm aperture at 5-cm distance from the object and a photomultiplier tube at a distance of 10 cm from this aperture. The advantage of a photomultiplier tube is the speed and sensitivity, so the modulation of a speckle can be detected real time at the US frequency and well within the speckle decorrelation time. The disadvantage is the small detection surface, which in turn reduces the number of tagged photons that can be detected, leading to small signal-to-noise ratio due to the influence of shot noise. In a nutshell: increasing the number n of speckle grains on the same single detector increases the random modulated signal standard deviation (signal of interest) as $n^{1/2}$ and the average power impinging the detector by n. If the detection is shot noise limited (that is rather unlikely to happen) the noise is proportional to $n^{1/2}$, and the signal-to-noise ratio is not increased by increasing the number of speckle grains on the detector. If the noise is linked to the laser fluctuations it is proportional to n and the signal-to-

noise ratio will decrease when increasing the number of speckle grains on the detector.

A parallel speckle detection technique was developed by Leveque et al.[38] Instead of a single detector element, a CCD camera is used in which the illumination pulses and the ultrasound are timed with a fixed phase delay. The system was designed to make speckle size comparable to the pixel size. The SNR is improved by averaging the signal from all CCD pixels, making it a larger detector surface. The major disadvantage of a CCD camera as a detector is the reduced frame rate, hence the intensity of a speckle cannot be followed in time at the US frequency. However, by recording the light intensity for different phases of the ultrasound, the modulated intensity and the unmodulated intensity can be estimated. This can be achieved by varying the delay between US and the start of the exposure of the camera. In the case of four-phase measurement the exposure time of the camera is up to one quarter of the US period time.

The signal S_i for each phase from Fig. 3 is given by:

$$S_1 = NT_0 \left[\frac{I_{dc}}{4} + \frac{\sqrt{2}}{2\pi} I_{ac} \cos(\phi_1) \right]$$
$$S_2 = NT_0 \left[\frac{I_{dc}}{4} + \frac{\sqrt{2}}{2\pi} I_{ac} \sin(\phi_1) \right]$$
$$S_3 = NT_0 \left[\frac{I_{dc}}{4} - \frac{\sqrt{2}}{2\pi} I_{ac} \cos(\phi_1) \right] \qquad (8)$$
$$S_4 = NT_0 \left[\frac{I_{dc}}{4} - \frac{\sqrt{2}}{2\pi} I_{ac} \sin(\phi_1) \right].$$

From these intensities the AC intensity and phase can be calculated using these relations:

$$I_{ac} = \frac{\pi}{NT_0\sqrt{2}} \sqrt{(S_1 - S_3) + (S_2 - S_4)^2}$$
$$\phi_1 = \arctan\left(\frac{S_2 - S_4}{S_1 - S_3}\right), \qquad (9)$$

where I_{ac} is the modulated part of the intensity for a single pixel, NT_0 the total integration time, and the phase of the acousto-optic signal. Li et al.[39] showed similar relations for two and three phases.
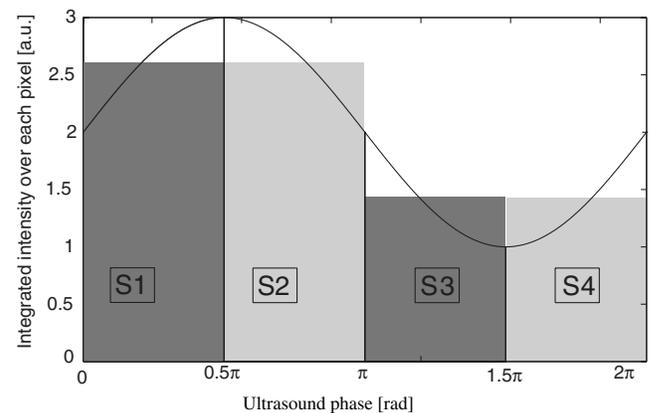

Fig. 3 Integrated light for each of the four quarters (S1, S2, S3, and S4) of the US period for a single pixel where the curved line denotes the instantaneous light intensity of this pixel.[18,38,40]

Parallel speckle detection is an efficient technique for detecting modulated light. However, this detection method is sensitive tospeckle decorrelation, which lowers the SNR by lowering the signal and increasing the noise.[18] Li et al.[41] showed a laser speckle contrast detection scheme that is less sensitive for speckle decorrelation when short integration times are used. The speckle contrast is defined as the standard deviation of the intensity in the pattern divided by the average intensity of this pattern.[42] Kothapalli et al.[43] tested their Monte Carlo implementation and measured with a speckle contrast setup; they further investigated the linear relation between speckle contrast and the local scattering coefficient at the US focus and found a good agreement between simulation and experiment.

4.2 Interferometric-Based Methods

Instead of following the intensity of the speckles in time domain, it is possible to filter out the modulated light with interferometers. The Fabry-Perot interferometer and Mach-Zehnder based techniques are used to detect, or select, only the modulated light at the US frequency. By optically removing noninteresting frequencies, the SNR should be increased.

Leutz et al.[7] used a Fabry-Perot interferometer in combination with a photomultiplier tube to detect photons with a frequency shift of 2.17 and 27.3 MHz from a laser source with a wavelength of 514.5 nm. To resolve this relative small frequency difference, they used a FP etalon (mirror reflectivity: 99.3%) with a mirror separation distance of 15 cm, obtaining a resolution of 12 MHz. The disadvantage of this technique is the great loss of signal photons due to the small *etendue* (the product of the solid angle and area of an aperture) when pinholes are used to select a parallel light beam with a certain frequency. However long-cavity[44] *confocal* Fabry-Perot interferometers are used, which have a high *etendue*. Double-pass confocal[45] Fabry-Perot interferometers are also used to separate the faint spectral line of the tagged photons from the strong untagged spectral line.

The heterodyne parallel speckle detection method adds a reference beam or local oscillator (LO) beam to the standard parallel speckle detection scheme,[46–48] making it a Mach-Zehnder interferometer, as depicted in Fig 4. This technique is shot-noise limited when using a large heterodyne reference intensity. When the signal beam is in phase with the reference beam the intensity on the detector is given by:[49]

$$I = I_s + I_{\text{ref}} + 2\sqrt{I_s I_{\text{ref}}}, \qquad (10)$$

where I is the detected intensity, I_s is the intensity of the signal beam and I_{ref} the intensity of the reference beam; the last term in this equation is the heterodyne gain.

The light in the sample arm is modulated as it propagates through the sample, and the reference arm is modulated with two acousto-optic frequency shifters (Bragg cells) or acousto-optic modulators. The speckle pattern from the sample interferes with the reference beam on the CCD camera, which is placed under a small tilt angle θ. The reference light with the modulated part of the sample generates a static speckle pattern, which can be detected by the CCD camera. Interference of the nonmodulated sample light with the reference light leads to a dynamic speckle pattern, which in the CCD image will be smeared out. The spatial frequency domain (k-space) of the recorded interference pattern reveals the level of the shot noise, the speckle decorrelation noise, and the tagged photons in different regions, due to spatial filtering associated with tilt angle θ. The sensitivity of this technique is limited by the shot noise of the reference light[46,47] and setup limitations such as dynamic range and sensitivity of the camera.From the four frames of the CCD array, representing the four phases of the reference beam, a four-phase complex signal can be calculated. This complex signal in k-space shows interesting properties. The heterodyne signal forms a narrow band of spatial frequencies at a position determined by tilt angle θ (region A in Fig 5), the decorrelation noise is relatively slow, and its fringes consists of the lower spatial frequencies (region B and C). The shot noise is represented by region D.

For example, the laser light is modulated at 85 MHz up and 80 MHz down with the use of two acousto-optic modulators. For practical reasons, two modulators are used instead of one at 5 MHz; that is the difference of both used modulators. The laser light inside the sample is modulated in the focus of a US transducer at 5 MHz.

This is known as single-phase detection; four-phase detection can be achieved by tuning one of the AO modulators slightly higher, 85.0000075 instead of 85 MHz. This way each next frame of the CCD array receives a reference beam with a phase shift of $\pi/2$ radians compared with the current frame assuming a frame rate of 30 frames per second.

The advantage of using multiple-phase detection is the higher SNR because the DC component is canceled out. All frames of the one to four phases should be taken within the speckle decorrelation time, making one or two phase imaging the better choice where this decorrelation time is short. Atlan et al.[48] give an equation to calculate the complex signal for an arbitrary number of phases.
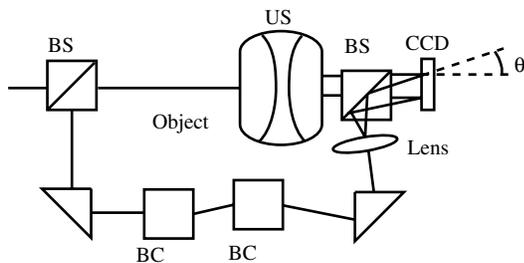

Fig. 4 Heterodyne parallel speckle detection, the light beam enters at the upper left beam splitter (BS) and illuminates the object. The ultrasound beam (US) is focused inside the object. The reference arm consists of twoprisms, two Bragg cells (BC), and a lens to expand the beam. Both arms are combined in the second beam splitter and the resulting interference pattern is detected by the CCD array.
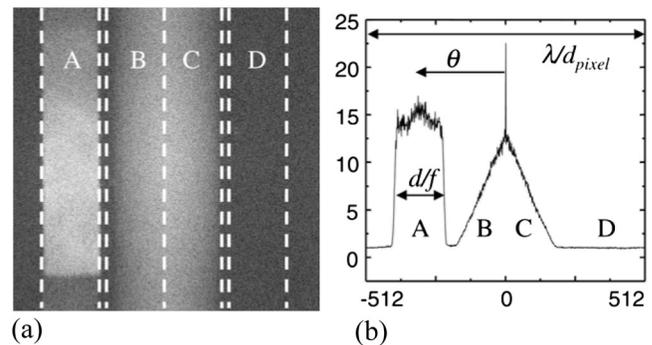

Fig. 5 k-space image (a) and column average of this image (b) with the regions: signal (A), decorrelation noise (B and C), and shot noise (D).[46]

Another technique uses the same heterodyne setup with the addition of a photo refractive crystal (PRC) in front of the detector. The principle is to store intensity and phase information of the speckle pattern inside a hologram and readout this hologram with a CCD. The advantage of this self-adapting wave-front holography is a larger *etendue* than most CCDsand possibly a larger SNR. Bloningen et al.[50,51] investigated the expected AO signal and phase shifts of the photons for photo-refractive-based detection by utilizing Monte Carlo simulations. They show that the average photon phase shift contains a DC phase shift, which is dominant over the usually used AC phase shift. This offers a possibility to compliment the AC data.

The crystal consists of a photorefractive material and thus has a refractive index that depends on the light intensity. The two beams, signal and reference, illuminate the crystal. The two interfering beams construct a three-dimensional (3-D) intensity profile in the crystal thus writing, using the photo refractive principle, a 3-D grating or hologram in the crystal within the response time. Typical response times are 100 μs for a $Al_{0.1}Ga_{0.9}As/GaAs$ multiple quantum well crystal (850-nm excitation wavelength),[52]0.3 to 100 ms for GaAs (1064 nm),[47,53–58] less than 10 ms for SPS:Te (790 nm)[59] and 150 ms for $Bi_{12}SiO_{20}$(532 nm).[51,60,61] Changes in the speckle pattern slower than this response time are not recorded, making the detection insensitive for slow speckle decorrelation. The photo-refractive effect selects only optical frequencies from the signal beam, which are close to the reference-beam frequency.

During readout of the hologram, the reference beam is diffracted by the holographic grating. This way the wavefront of the reference beam is shaped in the signal wavefront, but now with a larger intensity. This constructed speckle pattern can be detected by a detector such as a CCD. Chi et al.[62] describes this two wave mixing process in more detail. Gross et al.[53] give a detailed description of detecting tagged light with a PRC.

This self-adapting wavefront holography is a promising technique, but the typical response time is too slow for *in vivo* use where the speckle decorrelation times (<1 ms) are in general much shorter than the crystal response time ($\sim$100 ms).[57]

4.3 Other Methods

Spectral hole burning (SHB) is another crystal-based technique developed by Li et al.[57,63] where the PRC is replaced by a SHB crystal. This technique has also a large *etendue* and is insensitive for speckle decorrelation. The crystal acts as a narrow optic bandpass filter where most optical frequencies are absorbed and only one specific frequency band is transmitted. The reference beam burns a spectral hole in the crystal at the same frequency as the tagged photons. The crystal is an inhomogeneously broadened optical absorber that can be modeled as a two-level system. The spectral line width is typically sub-MHz when cryogenically cooled and depends on the intensity of the reference beam. During the burning process only the crystal ions inside the crystal that are sensitive for this specific optical frequency are excited from the ground state. This makes the crystal transparent for this optical frequency, the nontagged photons are absorbed by the crystal.

After burning the spectral hole, the reference beam is switched off and the signal beam is switched on, the tagged photons can be detected by a photo detector such as a CCD. The cryogenic cooling ($\sim$4 K) is the main disadvantage of this technique.

5 Resolution

The lateral resolution of acousto-optic imaging is obtained by focusing the ultrasound, and its size is comparable with the width of the US focus when the weight of the unfocused part does not play a major role. The axial resolution is worse than the lateral resolution due to the elongated focus of the ultrasound transducer (Rayleigh length).

The axial resolution can be improved in several ways by changing frequency, amplitude, or phase in time in order to get a resolution equivalent to the pulse-echo in US tomography.

The first method that was implemented is the frequency sweep technique.[64,65] In this method the ultrasound transducer generates a short chirped signal. The light along the acoustic axis is modulated with a different frequency for each depth. By using the Fourier transform on the detected signal, information in the axial direction is retrieved. Yao et al.[65] combined this chirp technique with a parallel detection scheme. They also showed that this technique does not rely purely on ballistic light by using an obliquely incident laser beam. Wang et al.[64] showed an axial resolution of approximately 1 mm;however, this resolution depends on the chirp rate. In chicken-breast tissue they achieved 4-mm resolution.[65]

Lesaffre et al.[58] showed a different approach by making the phase of the US and the optical illumination random. Both use the same data set of typical 512 random phases with each of these phases set to either 0 or π. This set of random phases has a typical period time 1 ms. The phase of the optical illumination is modulated with a delay τ relative to the modulation of the US. At a distance of τ times the speed of sound along the acoustic axis, both the optical illumination and US phase are correlated. Therefore only tagged photons from this position are detected using the heterodyne detection scheme with a photo refractive GaAs crystal. The resolution in the axial direction depends on the speed of sound and the time it takes to change phase, which in this case is (1 ms/512 $\approx$ 2 μs) roughly 3 mm. Gross et al. give more theoretical background[66] in regarding this technique.

A third method to increase the axial resolution uses short US pulses.[44,48,51,67] These pulses consist of a few US cycles and thus modulate the light only locally in the axial direction. The US pulse reaches the point of interest after time $t = z/c$, where z is the distance from the transducer and the point of interest and c the speed of sound (SOS). At this time (t) the sample is illuminated with pulse duration τ, and the modulated photons are recorded. The minimally resolvable size in the axial direction depends linearly on the SOS and pulse duration, assuming a short enough light pulse. Achieving high resolution thus requires short US pulses. The smaller the pulse duration, the bigger the spread of acoustic energy in the frequency domain. Detection schemes, which are only sensitive for a single frequency, require a longer US burst and thus a smaller US bandwidth to optimize the SNR.[67] Atlan et al.[48] used an US burst of 3 μs and the axial resolution is 5 mm.

Li et al.[68] investigated the influence of amplitude modulated US on the speckle contrast in a parallel detection setup. In this case the US amplitude was modulated with a 250-Hz-to-16-KHz cosine envelope. They show that amplitude modulated US can outperform continuous wave US in signal strength. Weng[69] investigated the relation between US pulse duration and amplitude on the AO signal and concluded that the imaging depth can be increased when reducing pulse duration and increasing the US peak amplitude.

Above methods all describe a way to improve the axial resolution by shaping the acoustic wave. The lateral resolution, however, is achieved by focusing the US transducer on the volume of interest. A different approach is suggested by Kuchment[70] where an unfocused US transducer is used. An unfocused transducer has spherical wavefronts in the far field. When the US transducer emits a small US wave train, a small circular shaped region is tagged. By repeating these measurements for different positions of the US transducer, a synthetic focus is constructed on the positions where these circular regions intersect. Another example of what could be seen as synthetic focusing is used by Li et al.[71] Sakadžić et al.[44] used tomography to achieve very high resolutions in the order of 100 μm.

Let us underline that whatever is the technique that led to reduce the resolution it has to involve signal variation shorter than the decorrelation time. This is obviously realized for short pluses but must also be done for other approaches such as the chirpsor the random sequences.

6 Applications of Acousto-Optic Imaging

6.1 Measuring Optical Properties

While it is still unknown what the measured quantity is in AO, its signal probably holds information on the local fluence rate. Lev and Sfez[12] showed the possibility of measuring the local fluence rate using AO between two optodes. This local fluence rate depends on position of illumination and detection and the optical properties distribution in the object such as the absorption coefficient. A map of the estimation of the optical absorption is obtained by scanning the US focus through the object and estimate the absorption coefficient for each position from the modulated fluence rate.[42] The AO signal is affected not only by optical absorption and scattering in the US focus but also in the rest of the object. Therefore quantitative estimation of the absorption coefficient requires the number of tagged and untagged photons and an algorithm that solves the inversion problem as in DOT.[30,33,54,72–74]

Gunadi and Leung[75] investigated the sensitivity of AO for the application of spectroscopy. From the spatial distribution of AO sensitivity they derived a penetration depth for AO of 14.8 mm for an intralipid solution with a μs' of 12 cm^{-1} and absorption of μa of 0.0235 cm^{-1}.

The absorption coefficient is in most cases dependent of the wavelength of the used light source, making functional imaging possible. For instance, chromophores such as hemoglobin and oxy-hemoglobin have distinct absorption spectra. This creates the possibility of determining the oxygenation levels of blood in biological tissues.[33]

6.2 Acousto-Optic Modulated Fluorescence

Fluorescence is often used to label particles and cells and enables the study of biological processes on the molecular and cellular level. However, light scattering makes it difficult to determine the origin of the fluorescent light in vivo. Efforts similar to DOT have to be made to perform optical tomography with fluorescent light.[76] Kobayashi et al.,[24] Hall et al.,[77] and Yuan et al.[76,78–81] investigated techniques to modulate and thereby localize this fluorescent light in turbid media.

The fluorescent light is noncoherent, and modulation has to come from modulation of optical properties of the sample.

The US field causes variation in the density and, consequently, induces a gradient of the refractive index based upon the localized pressure variations in the medium. On these gradients the light is deflected, which leads to variations in photon density in the fluorophores (mechanism 6 in Fig. 2), therefore the intensity of the fluorescence is modulated. Also, the scattering coefficient is modulated (mechanism 5), which causes fluorescence intensity modulation by variation of the photon density distribution.[24]

Yuan et al.[76,78–81] investigated the combination of fluorescence with AO and derived a mathematical model. They proposed two mechanisms that can explain the modulation of fluorescence. The first mechanism for low concentrations is similar to the explanation of Kobayashi et al.,[24] the excitation light is modulated and thus also the fluorescent light. For high concentrations, they propose a modulation in quenching rate and thus in detected intensity. At high concentrations the variation in distance between fluorophores leads to variations in quenching, giving a modulation of fluorescence that is inverted compared to lower concentrations where quenching is absent. The signal strength found by Yuan[80] shows a linear relation with the applied voltage on the ultrasound transducer, which is usually linear with the US pressure, and the signal was much weaker than found by Kobayashi et al.

Yuan et al. used a photo-multiplier tube to detect the modulation of the fluorescence and found that this signal depends quadratic on the acoustic pressure. Hall et al.[77] showed a parallel detection scheme to detect the modulation in fluorescence by modulating the gain of the CCD with the US frequency. The phase difference between the US and CCD gain modulation was 0 and 180 deg.

6.3 Acousto-Optic Assisted Elastograpy

AO elastography is an imaging modality for quantifying mechanical properties. Kirkpatrick et al.[82] stimulated tissue with a low frequency acoustic force (1 to 5 Hz), which induces a strain. The surface of the tissue, in their case the skin, will give a dynamic shift in the speckle pattern in the back-reflected laser light with this low frequency. The stiffer the material, the less shift in the speckle pattern is observed.

Bossy et al.[83] and Daoudi et al.[84] used a different approach to measure the elasticity of a material by use of AO.

A high-intensity US burst is focused into the object on the region of interest. Inside the focus a shear wave is generated that radiates away from the focal point with a speed of typically 1 to 2 mm/ms, which depends on the viscoelastic properties of the medium. This low speed causes a speckle decorrelation on ms time scale in transverse direction. This technique has a lateral resolution in the order of mm and is not limited to use at the surface. Li et al.[85] showed that by using the acoustic radiation force the resolution of a measurement can be increased by 40% to 110%. Sing et al.[86] used two transducers, which caused a beat and shear wave frequency of 250 Hz. This low frequency shear wave was detectable with a speckle contrast measurement.

6.4 Acousto-Optic Assisted Light Focusing in Turbid Media

Xu et al.[87] presented another detection technique called time-reversed ultrasonically encoded (TRUE) optical focusing based of a PRC used as a phase-conjugate mirror. The setup uses three arms: one signal arm where the object is located and two reference arms. The first reference arm is used for the

creation of the hologram inside the PRC; the second illuminates the crystal from the opposite direction. By the hologram inside the crystal, the light is focused inside the object with the focal point inside the US focus region. This increases the local fluence at the US focus; in the future one can expect a significant improvement of the light level at the focus if the phase conjugate mirror exhibits a noticeable gain. This method makes AO the only technique that can create a guide star, which makes direct focusing of light possible in turbid media. Inside the US focus, this light is tagged and detected outside the medium. A second benefit from using this phase conjugate PRC setup is the improved spatial resolution with a factor of $\sqrt{2}$.

6.5 Ex Vivo and In Vivo Experiments

Various groups report measurements *ex* and *in vivo* with the use of AO. Kim et al.[13] showed an image of chicken breast tissue with an embedded methylene-blue-dyed sentinel lymph node. Another *ex vivo* measurement on chicken breast is performed by Hisaka and Sasakura;[88] they also used a reflection mode AO setup. Both experiments show the feasibility of a reflection mode AO setup on real tissue.

Kothapalli and Wang[89] embedded mouse and rat blood vessels in tissue mimicking phantom material at a depth of 3 mm and imaged these vessels with an AO microscopy setup. They also tested the AO microscopy setup on a phantom.[90] These experiments were performed *ex vivo* and show the possibility of measurements on tissue and have thus the correct scattering and absorption coefficients. Recently Lai et al.[91] showed an *ex vivo* measurement on an HIFU induced lesion and compared the result with B-mode ultrasound. They concluded that AO sensing can follow the formation of the induced lesion in real time, and for noncavitating lesions AO gives a more robust signal compared with B-mode ultrasound. Murray et al.[92] further investigated the changes in AO response of *ex vivo* chicken breast while elicited by a high-intensity ultrasound field. They concluded that with the use of AO it is possible to probe in real time the formation of a HIFU lesion.

In vivo experiments are performed by Lev et al.[93,94] They demonstrate that *ex vivo* measurements suffer much less from speckle decorrelation than *in vivo* experiments. Further, they demonstrated the first AO tomography measurements on both mice and humans.

7 Discussion and Outlook

Tagged photons can be detected with several techniques. The photodetectors, which are fast enough to match the frequency of the US, have, in general, small detector surfaces. To avoid loss of SNR, averaging over multiple speckles must be avoided. These properties lead to a small *etendue* and thus a low count of tagged photons. CCD arrays can detect light from thousands of speckles in parallel and collect more light, resulting in an expected higher SNR. Unfortunately, these detectors are slow, therefore a lock-in detection is used, and only a few phases of the US are sampled.

Compared to untagged photons, tagged photons have a shifted optical frequency. Several spectrometer-based techniques are described in literature and have the advantage of greater stability. Small fluctuations in power, wavelength, and phase are canceled out assuming a long coherence length of the laser light. By using heterodyne detection it is possible to distinguish between speckle decorrelation by Brownian motion, shot-noise level, and the signal strength. Heterodyne detection

also amplifies the signal optically to rise the signal above the level of the untagged photons.

PRC-based detection has a large *etendue* and the advantage of signal amplification. The disadvantage is the low response time of typical crystals, which makes it sensitive to speckle decorrelation. Spectral hole burning or confocal Fabry-Perot filters are insensitive to speckle decorrelation because they act as band pass filters and have the largest *etendue*.[57] Crystal must be cryogenically cooled in order to achieve a narrow bandwidth in the MHz range, and Fabry-Perot need to be stabilized with a high precision feedback loop and isolated from mechanical vibrations.

To achieve high resolution in lateral direction, an ultrasound transducer with a small focal spot size is required. To achieve good axial resolution the frequency, phase and/or amplitude of the ultrasound can be made time dependent. This way only in a small part of the column, defined by the US beam, the light is tagged with these specific properties. The main advantage of giving a short US burst (amplitude) is the high acoustic peak pressure and therefore large modulation of light. The advantage of giving a chirped US pulse is the amount of information that is received in a single measurement; instead of measuring a single point, information can be extracted along the line in the US propagation direction.

The major challenges in *in vivo* AO applications are speckle decorrelation and low light levels. In general a detection method that detects as many tagged photons as possible is desired to obtain a good SNR. One strategy would be longer integration times; however, *in vivo* speckle decorrelation occurs on time scales of 1 ms. Most PRC have a response time orders of magnitude longer than 1 ms and are therefore not suitable for *in vivo* measurements. CCD-based techniques must acquire all light within the speckle decorrelation time, increasing shot noise and decreasing SNR. Spectral hole burning and Fabry-Perot interferometers are insensitive for speckle decorrelation and thus have none of these disadvantages; however, it is difficult to make sufficiently large *etendue*. Therefore these techniques are likely to be most suitable for *in vivo* imaging. Another more fundamental aspect in the introduction of acousto-Op. for *in vivo* application is the uncertainty regarding the exact information that is provided by AO. Although the spatial resolution of AO is potentially good, the property that it samples is related to the local fluence rate, which usually exhibits variations over a larger spatial scale. This aspect can be investigated using the new technologies that have been described in this review.

References

1. M. Heijblom et al. "Imaging tumor vascularization for detection and diagnosis of breast cancer," *Techn. Canc. Re. Treat.* **10**(6), 607–623 (2011).
2. F. A. Duck, *Physical Properties of Tissue*, Academic Press, London (1990).
3. C. G. A. Hoelen and F. F. M. de Mul, "A new theoretical approach to photoacoustic signal generation," *J. Acoust. Soc. Am.* **106**(2), 695–706 (1999).

4. H. F. Zhang et al. "Functional photoacoustic microscopy for high-resolution and noninvasive *in vivo* imaging," *Nat. Biotechnol.* **24**(7), 848–851 (2006).

5. S. Manohar et al., "The twente photoacoustic mammoscope: system overview and performance," *Phys. Med. Biol.* **50**(11), 2543–2557 (2005).

6. F. A. Marks, H. W. Tomlinson, and G. W. Brooksby, "Comprehensive approach to breast cancer detection using light: photon localization by ultrasound modulation and tissue characterization by spectral discrimination," *Proc. SPIE* **1888**, 500–510 (1993).

7. W. Leutz and G. Maret, "Ultrasonic modulation of multiply scattered-light," *Phys. B-Cond. Matt.* **204**(1–4) 14–19 (1995).

8. L. H. Wang, S. L. Jacques, and X. M. Zhao, "Continuous-wave ultrasonic modulation of scattered laser-light to image objects in turbid media," *Optic. Lett.* **20**(6), 629–631 (1995).

9. D. Dolfi and F. Micheron, "Imaging process and system for transillumination with photon frequency marking," International Patent WO 1989/000278 (1989).

10. L. H. V. Wang, "Ultrasound-mediated biophotonic imaging: a review of acousto-optical tomography and photo-acoustic tomography," *Disease Markers* **19**(2–3), 123–138 (2003).

11. D. S. Elson et al., "Ultrasound-mediated optical tomography: a review of current methods," *Inter. Fo.* **1**(4), 632–648 (2011).

12. A. Lev and B. G. Sfez, "Direct, noninvasive detection of photon density in turbid media," *Optic. Lett.* **27**(7), 473–475 (2002).

13. C. Kim et al., "Ultrasound-modulated optical tomography in reflection mode with ring-shaped light illumination," *J. Biomed. Optic.* **14**(2), 024015 (2009).

14. A. Lev, Z. Kotler, and B. G. Sfez, "Ultrasound tagged light imaging in turbid media in a reflectance geometry," *Optic. Lett.* **25**(6), 378–380 (2000).

15. H. B. Fu et al., "Ultrasound-modulated optical tomography in reflective and coaxial configuration," *Chinese Phys. Lett.* **20**(12), 2165–2168 (2003).

16. E. Granot et al., "Detection of inhomogeneities with ultrasound tagging of light," *J. Optical Soc. Am. A—Optic. Image Sci. Vis.* **18**(8), 1962–1967 (2001).

17. G. Yao and L. H. V. Wang, "Theoretical and experimental studies of ultrasound-modulated optical tomography in biological tissue," *Appl. Optic.* **39**(4), 659–664 (2000).

18. S. Lévêque-Fort, "Three-dimensional acousto-optic imaging in biological tissues with parallel signal processing," *Appl. Optic.* **40**(7), 1029–1036 (2001).

19. F. Martelli, *Light Propagation Through Biological Tissue and Other Diffusive Media: Theory, Solutions, and Software*, SPIE Press, Bellingham, Wash. (2010).

20. L. H. V. Wang, "Mechanisms of ultrasonic modulation of multiply scattered coherent light: a Monte Carlo model," *Optic. Lett.* **26**(15), 1191–1193 (2001).

21. L. H. V. Wang, "Mechanisms of ultrasonic modulation of multiply scattered coherent light: an analytic model," *Phys. Rev. Lett.* **8704**(4), 043903 (2001).

22. S. Sakadzic and L. V. Wang, "Modulation of multiply scattered coherent light by ultrasonic pulses: an analytical model," *Phys. Rev. E* **72**(3), 036620 (2005).

23. K. B. Krishnan et al., "A theory for the ultrasound modulation of incoherent light in turbid medium," *Proc. SPIE* **6009**, 60090V (2005).

24. M. Kobayashi et al., "Fluorescence tomography in turbid media based on acousto-optic modulation imaging," *Appl. Phys. Lett.* **89**(18), 181102 (2006).

25. G. D. Mahan et al. "Ultrasonic tagging of light: theory," *Proc. Natl. Acad. Sci. U. S. A.* **95**(24), 14015–14019 (1998).

26. S. Sakadzic and L. H. V. Wang, "Ultrasonic modulation of multiply scattered coherent light: an analytical model for anisotropically scattering media," *Phys. Rev. E* **66**(2) (2002).

27. R. Zemp, S. Sakadzic, and L. V. Wang, "Stochastic explanation of speckle contrast detection in ultrasound-modulated optical tomography," *Phys. Rev. E* **73**(6), 061920 (2006).

28. M. Allmaras and W. Bangerth, "Reconstructions in Ultrasound Modulated Optical Tomography," (9 April 2010).

29. S. Sakadzic and L. H. V. Wang, "Correlation transfer equation for ultrasound-modulated multiply scattered light," *Phys. Rev. E* **74**(3) (2006).

30. S. Sakadzic and L. H. V. Wang, "Correlation transfer and diffusion of ultrasound-modulated multiply scattered light," *Phys. Rev. Lett.* **96**(16) (2006).

31. L. V. Wang and S. Sakadzic, "Correlation transfer equation for multiply scattered light modulated by an ultrasonic pulse," *J. Opt. Soc. Am. A—Optic. Image Sci. Vis.* **24**(9), 2797–2806 (2007).

32. J. Laufer et al., "*In vitro* measurements of absolute blood oxygen saturation using pulsed near-infrared photoacoustic spectroscopy: accuracy and resolution," *Phys. Med. Biol.* **50**(18), 4409–4428 (2005).

33. A. Bratchenia, R. Molenaar, and R. P. H. Kooyman, "Feasibility of quantitative determination of local optical absorbances in tissue-mimicking phantoms using acousto-optic sensing," *Appl. Phys. Lett.* **92**(11), 113901 (2008).

34. M. S. Singh et al., "Assessment of ultrasound modulation of near infrared light on the quantification of scattering coefficient," *Med. Phys.* **37**(7), 3744–3751 (2010).

35. J. M. Elazar and O. Steshenko, "Doppler effect's contribution to ultrasonic modulation of multiply scattered coherent light: Monte Carlo modeling," *Optic. Lett.* **33**(2), 131–133 (2008).

36. C. H. Kim and L. V. Wang, "Multi-optical-wavelength ultrasound-modulated optical tomography: a phantom study," *Optic. Lett.* **32**(16), 2285–2287 (2007).

37. T. S. Leung and S. Powell, "Fast Monte Carlo simulations of ultrasound-modulated light using a graphics processing unit," *J. Biomed. Optic.* **15**(5), 055007 (30 September 2010).

38. S. Leveque et al., "Ultrasonic tagging of photon paths in scattering media: parallel speckle modulation processing," *Optic. Lett.* **24**(3), 181–183 (1999).

39. J. Lie and L. V. Wang, "Methods for parallel-detection-based ultrasound-modulated optical tomography," *Appl. Optic.* **41**(10), 2079–2084 (2002).

40. J. Selb et al., "3-D acousto-optic modulated-speckle imaging in biological tissues," *Comptes Rendus De L Academie Des Sciences Serie Iv Physique Astrophysique* **2**(8), 1213–1225 (2001).

41. J. Li, G. Ku, and L. H. V. Wang, "Ultrasound-modulated optical tomography of biological tissue by use of contrast of laser speckles," *Appl. Optic.* **41**(28), 6030–6035 (2002).

42. A. Bratchenia et al., "Millimeter-resolution acousto-optic quantitative imaging in a tissue model system," *J. Biomed. Optic.* **14**(4), 034031 (2009).

43. S. R. Kothapalli et al., "Imaging optically scattering objects with ultrasound-modulated optical tomography," *Optic. Lett.* **32**(16), 2351–2353 (2007).

44. S. Sakadzic and L. H. V. Wang, "High-resolution ultrasound-modulated optical tomography in biological tissues," *Optic. Lett.* **29**(23), 2770–2772 (2004).

45. G. Rousseau, A. Blouin, and J. P. Monchalin, "Ultrasound-modulated optical imaging using a high-power pulsed laser and a double-pass confocal Fabry-Perot interferometer," *Optic. Lett.* **34**(21), 3445–3447 (2009).

46. M. Gross, P. Goy, and M. Al-Koussa, "Shot-noise detection of ultrasound-tagged photons in ultrasound-modulated optical imaging," *Optic. Lett.* **28**(24), 2482–2484 (2003).

47. M. Gross et al., "Detection of the tagged or untagged photons in acousto-optic imaging of thick highly scattering media by photorefractive adaptive holography," *Euro. Phys. J. E* **28**(2), 173–182 (2009).

48. M. Atlan et al., "Pulsed acousto-optic imaging in dynamic scattering media with heterodyne parallel speckle detection," *Optic. Lett.* **30**(11), 1360–1362 (2005).

49. K. Creath, "Phase-shifting speckle interferometry," *Appl. Optic.* **24**(18), 3053–3058 (1985).

50. F. J. Blonigen et al., "Computations of the acoustically induced phase shifts of optical paths in acoustophotonic imaging with photorefractive-based detection," *Appl. Optic.* **44**(18), 3735–3746 (2005).

51. T. W. Murray et al., "Detection of ultrasound-modulated photons in diffuse media using the photorefractive effect," *Optic. Lett.* **29**(21), 2509–2511 (2004).

52. M. Tziraki et al., "Short-coherence photorefractive holography in multiple-quantum-well devices using light-emitting diodes," *Appl. Phys. Lett.* **75**(10), 1363–1365 (1999).

53. M. Gross et al., "Theoretical description of the photorefractive detection of the ultrasound modulated photons in scattering media," *Optic. Ex.* **13**(18), 7097–7112 (2005).

54. P. X. Lai, R. A. Roy, and T. W. Murray, "Quantitative characterization of turbid media using pressure contrast acousto-optic imaging," *Optic. Lett.* **34**(18), 2850–2852 (2009).

55. F. Ramaz et al., "Photorefractive detection of tagged photons in ultrasound modulated optical tomography of thick biological tissues," *Optic. Ex.* **12**(22), 5469–5474 (2004).

56. G. Rousseau, A. Blouin, and J. P. Monchalin, "Ultrasound-modulated optical imaging using a powerful long pulse laser," *Optic. Ex.* **16**(17), 12577–12590 (2008).

57. Y. Z. Li et al.,"Pulsed ultrasound-modulated optical tomography using spectral-hole burning as a narrowband spectral filter," *Appl. Phys. Lett.* **93**(1), 011111 (2008).

58. M. Lesaffre et al., "Acousto-optical coherence tomography using random phase jumps on ultrasound and light," *Optic. Ex.* **17**(20), 18211–18218 (2009).

59. S. Farahi et al.,"Photorefractive acousto-optic imaging in thick scattering media at 790 nm with a Sn2P2S6:Te crystal," *Optic. Lett.* **35**(11), 1798–1800 (2010).

60. E. Bossy et al.,"Fusion of conventional ultrasound imaging and acousto-optic sensing by use of a standard pulsed-ultrasound scanner," *Optic. Lett.* **30**(7), 744–746 (2005).

61. L. Sui et al.,"Imaging in diffuse media with pulsed-ultrasound-modulated light and the photorefractive effect," *Appl. Optic.* **44**(19), 4041–4048 (2005).

62. M. J. Chi, J. P. Huignard, and P. M. Petersen, "A general theory of two-wave mixing in nonlinear media," *J. Opt. Soc. Am. B-Opt. Phys.* **26**(8), 1578–1584 (2009).

63. Y. Z. Li et al., "Detection of ultrasound-modulated diffuse photons using spectral-hole burning," *Optic. Ex.* **16**(19), 14862–14874 (2008).

64. L. H. V. Wang and G. Ku, "Frequency-swept ultrasound-modulated optical tomography of scattering media," *Optic. Lett.* **23**(12), 975–977 (1998).

65. G. Yao, S. L. Jiao, and L. V. Wang, "Frequency-swept ultrasound-modulated optical tomography in biological tissue by use of parallel detection," *Optic. Lett.* **25**(10), 734–736 (2000).

66. M. Gross et al."Theoretical study of acousto-optical coherence tomography using random phase jumps on ultrasound and light," *J. Opt. Soc. Am. A-Optic. Image Sci. Vis.* **28**(7), 1436–1444 (2011).

67. A. Lev and B. G. Sfez, "Pulsed ultrasound-modulated light tomography," *Optic. Lett.* **28**(17), 1549–1551 (2003).

68. R. Li et al., "Parallel detection of amplitude-modulated, ultrasound-modulated optical signals," *Optic. Lett.* **35**(15), 2633–2635 (2010).

69. C. C. Weng, "Noninvasive determination of optical properties of scattering media," *Euro. Phys. J. App. Phys.* **50**(3), 31401 (2010).

70. P. Kuchment and L. Kunyansky, "Synthetic focusing in ultrasound modulated tomography," *In. Probl. Imag.* **4**(4), 665–673 (2010).

71. J. Li and L. H. V. Wang, "Ultrasound-modulated optical computed tomography of biological tissues," *Appl. Phys. Lett.* **84**(9), 1597–1599 (2004).

72. G. Bal and J. C. Schotland, "Inverse scattering and acousto-optic imaging," *Phys. Rev. Lett.* **104**(4), 043902 (2010).

73. A. Bratchenia et al., "Acousto-optic-assisted diffuse optical tomography," *Optic. Lett.* **36**(9), 1539–1541 (2011).

74. A. Bratchenia, R. Molenaar, and R. Kooyman, "Towards quantitative acousto-optic imaging in tissue," *Laser Phys.* **21**(3), 1–7 (2011).

75. S. Gunadi and T. S. Leung, "Spatial sensitivity of acousto-optic and optical near-infrared spectroscopy sensing measurements," *J. Biomed. Optic.* **16**(12), 127005 (2011).

76. B. H. Yuan, J. Gamelin, and Q. Zhu, "Mechanisms of the ultrasonic modulation of fluorescence in turbid media," *J. Appl. Phys.* **104**(10), 103102 (2008).

77. D. J. Hall, U. Sunar, and S. Farshchi-Heydari, "Quadrature detection of ultrasound-modulated photons with a gain-modulated, image-intensified, CCD camera," *Open Optic. J.* **2**(1), 75–78 (2008).

78. B. H. Yuan, "Ultrasound-modulated fluorescence based on a fluorophore-quencher-labeled microbubble system," *J. Biomed. Optic.* **14**(2), 024043 (2009).

79. B. H. Yuan, "Sensitivity of fluorophore-quencher labeled microbubbles to externally applied static pressure," *Med. Phys.* **36**(8), 3455–3469 (2009).

80. B. H. Yuan and Y. A. Liu, "Ultrasound-modulated fluorescence from rhodamine B aqueous solution," *J. Biomed. Optic.* **15**(2), 021321 (2010).

81. B. H. Yuan et al., "Microbubble-enhanced ultrasound-modulated fluorescence in a turbid medium," *Appl. Phys. Lett.* **95**, 181113 (18) (2009).

82. S. J. Kirkpatrick et al., "Imaging the mechanical stiffness of skin lesions by in vivo acousto-optical elastography," *Optic. Ex.* **14**(21), 9770–9779 (2006).

83. E. Bossy et al.,"Transient optoelastography in optically diffusive media," *Appl. Phys. Lett.* **90**(17), 174111 (2007).

84. K. Daoudi, A. C. Boccara, and E. Bossy, "Detection and discrimination of optical absorption and shear stiffness at depth in tissue-mimicking phantoms by transient optoelastography," *Appl. Phys. Lett.* **94**(15), 154103 (2009).

85. R. Li et al.,"Effects of acoustic radiation force and shear waves for absorption and stiffness sensing in ultrasound modulated optical tomography," *Optic. Ex.* **19**(8), 7299–7311 (2011).

86. M. S. Singh, K. Rajan, and R. M. Vasu, "Estimation of elasticity map of soft biological tissue mimicking phantom using laser speckle contrast analysis," *J. Appl. Phys.* **109**(10), 104704 (2011).

87. X. Xu, H. Liu, and L. V. Wang, "Time-reversed ultrasonically encoded optical focusing into scattering media," *Nat. Photon.* **5**(3), 154–457 (2011).

88. M. Hisaka and Y. Sasakura, "Light scattering characteristics of biological tissues in coaxial ultrasound-modulated optical tomography," *Jap. J. Appl. Phys.* **48**(6), 067002 (2009).

89. S. R. Kothapalli and L. H. V. Wang, "*Ex vivo* blood vessel imaging using ultrasound-modulated optical microscopy," *J. Biomed. Optic.* **14**(1), 014015 (2009).

90. S. R. Kothapalli and L. H. V. Wang, "Ultrasound-modulated optical microscopy," *J. Biomed. Optic.* **13**(5), 054046 (2008).

91. P. X. Lai et al.,"Real-time monitoring of high-intensity focused ultrasound lesion formation using acousto-optic sensing," *Ultrasound Med. Biol.* **37**(2), 239–252 (2011).

92. T. Murray, P. Lai, and R. Roy, "Measuring tissue properties and monitoring therapeutic responses using acousto-optic imaging," *Ann. Biomed. Eng.* **40**(2), 474–485 (2012).

93. A. Lev et al.,"Ultrasound-modulated light tomography assessment of osteoporosis," *Optic. Lett.* **30**(13), 1692–1694 (2005).

94. A. Lev and B. Sfez, "*In vivo* demonstration of the ultrasound-modulated light technique," *J. Opt. Soc. Am. A-Opt. Image Sci. Vis.* **20**(12), 2347–2354 (2003).